Chapter 4

Laser Based Fabrication of Graphene

Kai Wang

Additional information is available at the end of the chapter

http://dx.doi.org/10.5772/55821

1. Introduction

Graphene, two dimensional (2D) carbon-carbon atoms arranged in a hexagonally honeycomb lattice structure, is the latest carbon (C) allotrope to be discovered. It has gained tremendous scientific research interests due to some unique properties, such as quantum hall effect and nearly ballistic electronic transportation in ambient.[1-4] These properties have stimulated intense activity among physicists, chemists and material scientists. Much research has focused on developing routs for the controllable growth of high quality graphene. Historically, graphene can be produced via micromechanical cleavage and SiC decomposition methods.[2, 5, 6] In order to meet even higher requirements, such as good crystallinity, less impurities and large area coverage, the present most successful fabrication technique focuses on chemical vapor deposition (CVD) on copper [5 - 8] Some other graphene growth methods include growth of graphene from solid carbon source, graphene synthesis by ion beam implantation, and graphene formation by decomposition of C_{60}, have also been reported in the recent years.[9, 10] Apart from these, pulsed laser deposition (PLD), which is one of the unique physical vapor deposition (PVD) methods, represents a completely new fabrication way in this field.

For many reasons, PLD is a versatile material fabrication technique. There are many laser parameters regarding sample preparation can be tuned in the PLD system, which have great influence on the sample qualities. First, for laser itself, the laser fluence, wavelength, repetition rate, and pulse duration can be altered. The second aspect includes target to substrate distance, background gas and pressure, and substrate temperature can be varied depending on certain requirements. Since with this technique the energy source, laser, is located outside the vacuum system, it is possible to adopt ultrahigh vacuum (UHV) as well as ambient conditions. It allows growing many kinds of materials; for example, oxides, nitrides, carbides, semiconductors, metals, superconductors, superlattice structures, and even fullerenes and polymers. The pulsed nature of PLD process even allows preparing complex polymer-metal compounds and

multylayers. For example, one of the promising realizations of the PLD system is to introduce oxygen to the chamber for oxides based fabrication. It is inevitable for achieving a sufficient amount of oxygen during film growth.

Until now, there have fewer studies on PLD based graphene growth. Indeed, such method used in graphene fabrication originates from the growth of carbon thin film by the PLD system. If a single carbon layer with aromatic ring structure in plane can be obtained, it gives a result of a single layer graphene. For the PLD method, the amorphous C layer can be easily deposited at room temperature. However, in order to fabricate C layer or graphene with a desirable crystalline quality by PLD, some additional conditions are required. For example, the substrate temperatures, vacuum level inside the PLD chamber, appropriate laser operation conditions (i.e. laser fluence and repetition rate) and the choice of catalytic metals. Wang, et. al. have demonstrated that few layer graphene that is bi-layer to multi-layer graphene can be fabricated on catalytic nickel (Ni) thin film by PLD system.[11] The number of graphene layers is found depending on the laser ablation time, and the crystallinity of the graphene depends on the substrate temperature during laser ablation. During the graphene formation, it involves several steps, such as C atoms adsorption, precipitation, segregation and recrystallization. All these processes happen due to the interaction between C atoms and metals. The formation of the graphene on the metal surfaces was first observed during the preparations of platinum (Pt) and ruthenium (Ru) single crystal surfaces. [12, 13]

In fact, the studies of the interaction of the C and the metals has a long history, however, the graphene fabricated by PLD method is realized in the recent years. By comparing with the conventional CVD method which usually involves high processing temperature (>1000 ^{o}C) and chemical reactive hydrocarbon gas flow, PLD can reach the same goal at relatively low temperatures and the C target is always in a solid form. Koh, et. al. have demonstrated that few layer graphene can be fabricated at 750 ^{o}C on a Ni plate (Figure 1).[14] Apart from the temperature issue, they also showed the cooling rate and laser energy are crucial in fabricating such graphene layers. Afterwards, Wang, et. al. did more systematic studies on the formation of the graphene on the Ni thin film. The significant contribution from their work is the number of graphene layer can be controlled by altering the number of the laser pulses (Figure 2). [11]

Apart from the demonstration of this PLD fabrication technique in this chapter, the characterizations and quantitative studies of graphene mainly rely on fast and non-destructive micro-Raman spectroscopy.[6, 15-17] In the past four decades, it has witnessed that Raman spectroscopy plays an important role in characterizing pyrolytic graphite, glassy carbon, graphitic foams, carbon fibers, nanographite ribbons, carbon nanotubes and fullerences. Owing to the presence of sp^2 bond graphene, Raman spectroscopy gives plenty of inspired information about crystallite size, the introduction of chemical impurities, the magnitude of the mass density, the optical energy gap, the elastic constants, the doping, defects, the crystal disorder, the strain, and the number of the graphene layers. With this respect, the discussion about PLD fabricated graphene here will provide a taste of the power of Raman spectroscopy.

http://dx.doi.org/10.5772/55821

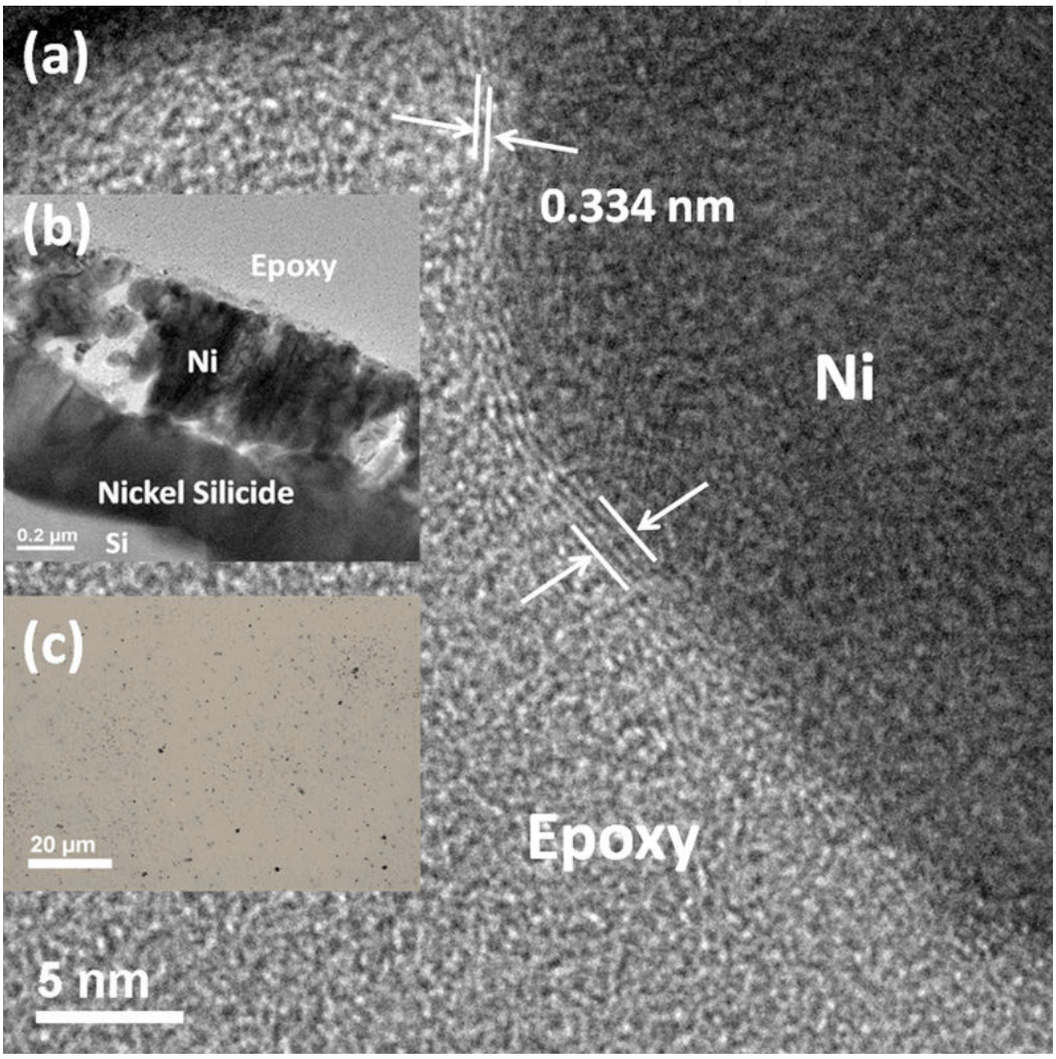

Figure 1. Crossing sectional TEM showing (a) the graphene layers above Ni. (b) Ni/nickel silicide/Si layered structure. Inset c is an overview optical image showing rather uniform coverage [ref. 13. figure 2].

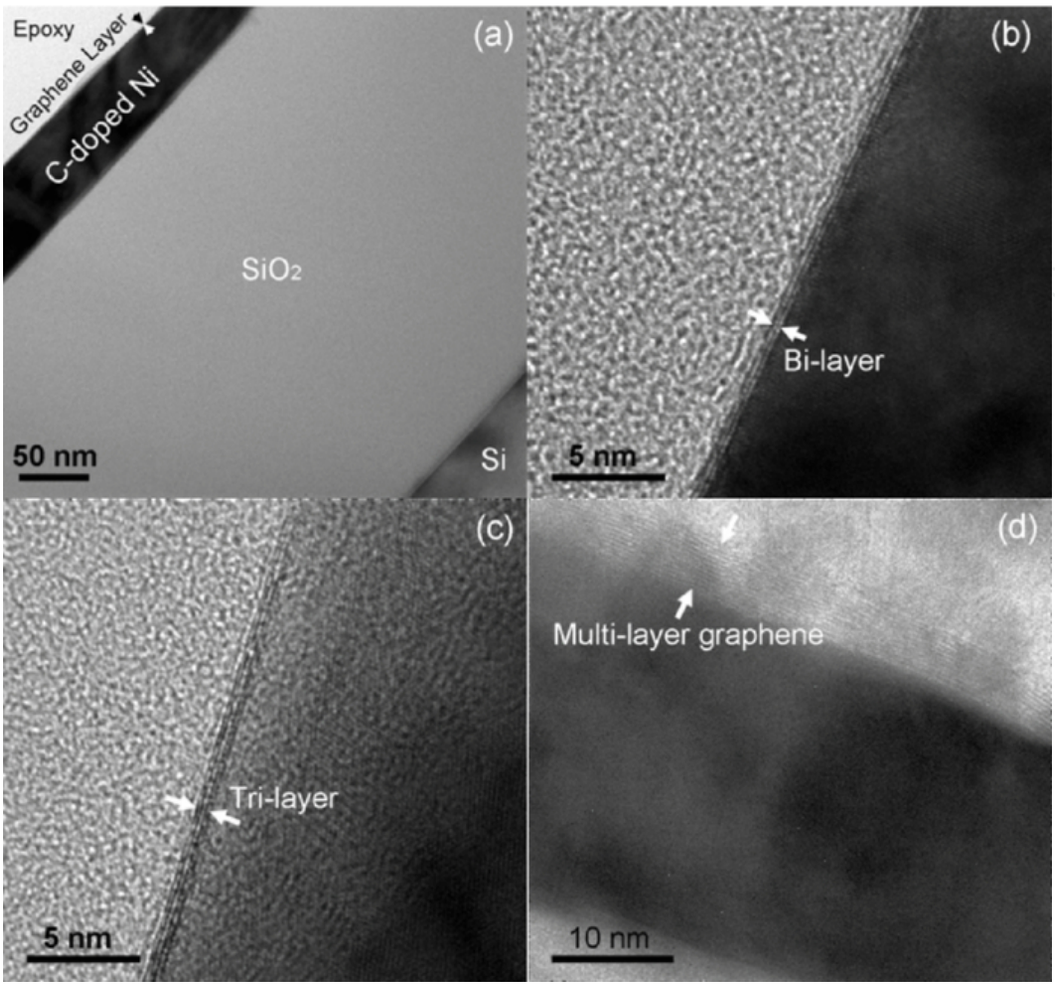

Figure 2. TEM characterization of PLD-grown graphene films. (a) Low magnification TEM image showing PLD-grown graphene on Ni thin film. High resolution TEM images for (b) bi-layer graphene, (c) tri-layer graphene and (d) multi-layer graphene.

2. Metal induced crystallization method

Metal induced crystallization method, also known as metal mediated or metal catalyzed crystallization method, is a crystalline growth technique to fabricate mono- or poly-crystalline materials via the interdiffusion, precipitation, segregation and recrystallization of two materials upon thermal annealing. One of them performs as the catalyst; it is usually a metal, such as aluminum (Al), gold (Au), platinum (Pt), nickel (Ni) and cobalt (Co); [11, 12, 18, 19] while the other is always chosen as a semiconductor material, such as germanium (Ge), and silicon (Si). This technique has been widely explored in the past, in particular for the poly-crystalline Si thin film based solar cell investigation.[20] It has been proposed and experimentally demonstrated in fabricating high crystalline quality and large area polycrystalline Si thin film on various kinds of substrates at low temperature. For both CVD and PVD method based graphene fabrications, metal induced crystallization method acts as a dominating role during

http://dx.doi.org/10.5772/55821

the graphitization process at elevated temperature. One way to realize this method in graphene growth is amorphous C layer can be easily changed to crystalline graphene layer based on thermal annealing process. Such process can be understood from figure 3.[21] This process utilizes solid phase sources of C. In this approach, the C is introduced in the amorphous phase with the Ni thin film forming bi-layer stack. Upon high temperature annealing, the C atoms from the a-C layer would dissolve into the Ni layer and be expelled from solution after cooling below the solid solubility limit. By comparing with previous studies about metal-induced Si crystallization, similar mechanism is involved. The driving force for crystallization is thermodynamic stability of the crystalline C and Si phases relative to the amorphous phase.

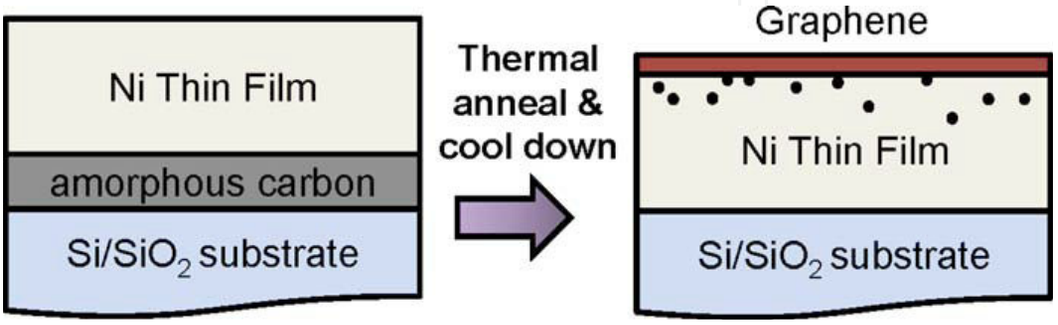

Figure 3. The process schematics for the metal-catalyzed crystallization of amorphous C to graphene by thermal annealing [ref. 19 figure 1].

3. An Introduction to pulsed laser deposition

3.1. Background of PLD

PLD is a thin film fabrication technique using high energy pulsed laser beam to bombard one or more targets at a certain vacuum pressure.[22, 23] The laser shooting areas of the targets experience the transition from the solid to the vapor phase, and subsequently been coated onto a substrate. This growth technique was first used by Smith and Turner in 1965 for the preparation of semiconductors and dielectric thin films.[24] It was further established by Dijkkamp and coworkers on high temperature superconductors in 1987.[25] Afterwards, this technique has been extensively optimized, investigated, and used in oxides, nitrides, carbides, metallic thin films and even organic polymers.[26]

3.2. PLD system setup

PLD is a form of physical vapor deposition (PVD). The system design is somewhat different from other PVD systems such as, thermal evaporation, electron beam evaporation, molecular beam epitaxial growth and magnetron sputter systems, because an external laser source is required. The useful range of laser wavelengths for thin films growth by PLD lies between 200 nm and 400 nm because most materials exhibit strong absorption in this spectral region. Therefore, most photon energies come from laser source can be absorbed by materials. Within this range, there

are few commercially available laser sources capable of easily delivering the high energy densities (1 J/cm^2), in relatively large areas (10 mm^2 or larger), which are required for PLD works. A homogenous uniform laser output is also important for high quality thin films fabrications. Most PLD systems work these days use excimer lasers, in which the lasing medium is a mixture of some reactive gases such as krypton (Kr), fluorine (F) and neon (Ne). It is also known that neodymium (Nd): YAG laser can also be used for graphite fabrication on Si substrate, but no one has demonstrated the fabrication of graphene using this laser source so far.

An experimental setup for a typical PLD system is shown in figure 4. It consists of two major components, one is the external laser source and another is the stainless steal vacuum chamber. The vacuum chamber can be placed direct facing the output laser pulse or be set at certain angles. For the latter case, a reflecting mirror is necessary. Inside the PLD chamber, a target and a substrate holder are aligned on the same line but are separated by a distance of 3 cm to 5 cm. Such distance range has been well experimentally confirmed for efficient laser ablation. When the incident focusing laser beam bombards the rotating target, the rise of the localized temperature causes vaporization of the material. It is a feature of plasma plume with high energetic species, for example, ions, electrons, atoms, molecules, clusters, particulates and molten globules. For an ideal PLD based thin films fabrication, people hope that the clusters, particulates and molten globules can be avoided. The film growths depend on several parameters, such as laser fluence, laser repetition rate, substrate temperature and vacuum level. By adjusting the number of laser pulses on the targets, different layers with controllable thicknesses can reach.

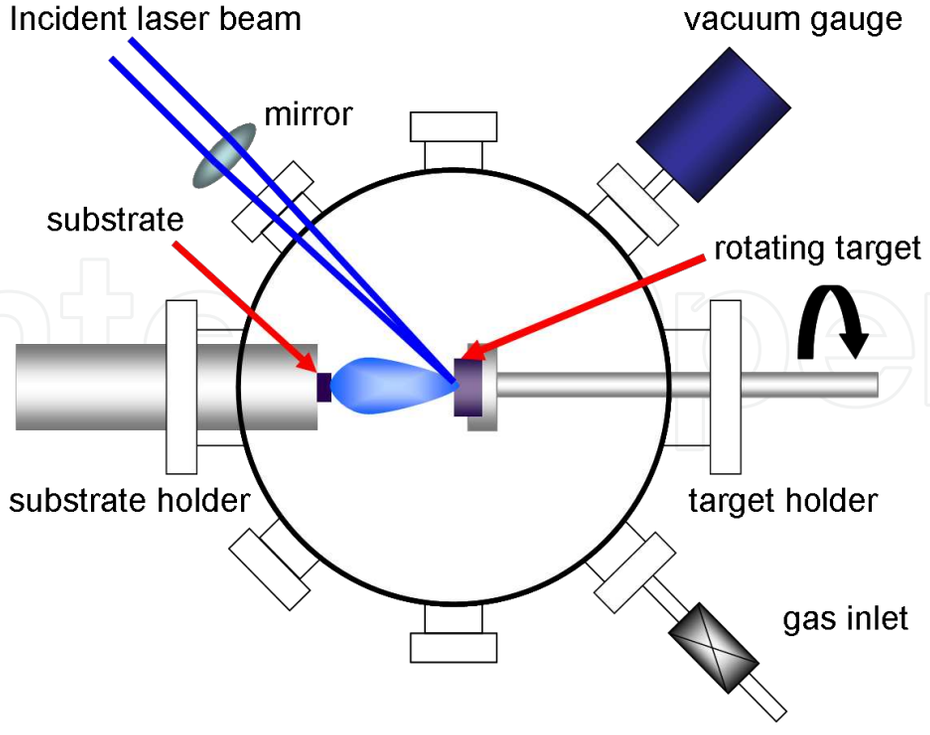

Figure 4. PLD system setup.

3.3. PLD technique in graphene fabrication

In a typical experiment for fabricating graphene layer via PLD, people can select different substrates based on certain requirements. For convenient purpose, we use 300nm SiO_2 coated Si as a typical example to illustrate this fabrication method (figure 5(a)). Furthermore, it is also a good candidate for making bottom gate graphene based field effect transistor (FET) due to the present of sufficient thick SiO_2 layer. Prior to the deposition, the substrate can be cleaned by the conventional chemical means. The fabrications for those metal thin films and C were carried out inside a stainless steal PLD chamber. The SiO_2/Si substrate was firmly attached onto a substrate holder, which is 4 cm in a distance to a PLD target holder. The laser beam can be guided to the target via a focusing lens. More details about the experimental condition can be found from reference 10. A schematic diagram which shows the graphene formation on a thin metal thin film is given in figure 5. The metal thin film is fabricated at room temperature (figure 5(b)). Without breaking the high vacuum, the substrate temperatures were rapidly increased to 650 °C and 600 °C. After the deposition of C (figure 5(c)), the samples were naturally cooled down to room temperature in an ultra-high vacuum. For some PLD systems, the cooling rate can also be controlled, for example by the flow of the liquid nitrogen or pass through the inert gas into the chamber. During this cooling process, the C atom will segregate from the C containing C-metal solid solution and form a continued layer on the topmost surface (figure 5(d)). This is due to the reduction of the solubility of C-metal solution. The metal which locates below graphene layer after fabrication is not a pure thin metal film anymore, because there are still sufficient amount of C atoms which participate the interdiffusion process remain and form C-metal eutectic alloy.

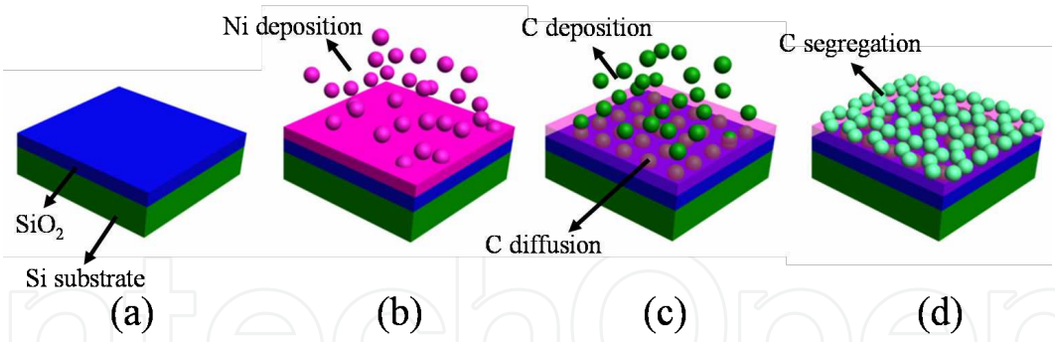

Figure 5. Schematic diagram shows metal-induced graphene formation process by PLD technique. (a) Preparation of SiO_2/Si substrate. (b) Ni thin film deposition at room temperature. (c) C deposition at elevated temperature. (d) Graphene formation at the topmost surface.

4. TEM and Raman spectroscopic studies

Figure 6 shows the Raman spectra for the carbon layers fabricated at 5 difference temperatures, 300 °C, 400 °C, 500 °C, 600 °C and 650 °C respectively on Ni thin film. In figure 6(a), there is no distinct peak can be observed for crystalline C phase. This indicates 300 °C is insufficiently to

obtain crystalline carbon layer on Ni thin film. As the deposition temperature for carbon increases, such as shown in figure 6(b) and (c), two remarkable bands tend to emerge at 1350 cm^{-1} and 1550 cm^{-1} respectively. Both of them represent disorder-induced (D) and graphitic (G) bands. For the one locates at 1350 cm^{-1}, its occurrence is due to the breathing mode of sp^2 atoms or A_{1g} symmetry in hexagonal graphitic rings. From both figure 6(b) and (c), a broad bandwidth of such D mode indicates the nonorganized C.[16] Thus, the large full width at half maximum (FWHM) of the D band yields the highly disordered characteristic of the C layer. This mode is forbidden in perfect graphite and become active in the presence of disorder. Furthermore, the D mode is dispersive and varies with photon excitation energy. Therefore, its intensity is strictly related with the presence of sixfold aromatic ring. As the atomic mechanism concerns, the rise of G band is ascribed to the in-plane stretching of the C-C bond in graphitic materials.[17] By comparing with the one of D mode, this one does not require the presence of sixfold ring so that it occurs at all pairs of sp^2 C sites. In the Raman spectra, the G band is due to the doubly degenerate zone center E_{2g} mode. The Raman spectroscopy is very sensitive to this strain effect in sp^2 C based materials. When the interaction between one graphene layer and substrate or another graphene layer is encountered, the induced strain is due to the modification of the C-C bond lengths and angles. As we can see from figure 6(d) and (e), further increase in the deposition temperature of C leads a clear distinguish of D and G bands. The relative intensity ratio of I_D to I_G has been significantly reduced at the deposition temperature of 650 ^oC for C. It results in the reduction of the crystalline defects. In addition, there is another band gradually become noticeable at 2700 cm^{-1}. It is the second order of zone-boundary phonons, but it has nothing to do with the G band. Because the Raman shift at this point is approximately doubled when comparing with the one of the D band, it is conventionally denoted as 2D or G′ band. Owing to the G′ band is the second order process associated with a phonon close to the K point in graphene, there has a strong dependence on any perturbation to the electronic and phonon structure of graphene. Therefore, G′ band plays an important role for differentiating single, bi- and few- layer graphene upon Raman spectroscopy.[6, 15] The results of the temperature dependence for C deposition suggests that 650 ^oC is an optimum temperature to fabricate the crystalline C layer on the Ni thin films by the PLD method in this experiment. Apart from Ni, it is also possible to fabricate graphene layer on a Co thin film. Figure 7 shows the temperature dependent graphene fabrication on the Co thin film. By comparing with figure 6, similar results were obtained for these two 3d transition metals.

Figure 8(a) shows the photographic image during graphene layer transferring process. The PLD made graphene transfer method is very similar to the one used in CVD method. A very thin protective poly[methyl methacrylate] (PMMA) layer was initially coated on the top of the graphene/Ni or Co/SiO_2/Si sample by spin coater. The catalytic Ni or Co can be etched away by chemical wet-etching, for instance using an aqueous HCL solution. In figure 8(a), After the Ni thin film was completely dissolved in $FeCl_3$ solution; a 1 × 1 cm^2 few layer graphene coated with the PMMA was detached from the Ni thin film and forms a free-standing layer in the HCl solution. The diluted HCl solution can be further utilized for removing the residual Ni flakes. Afterward, the few-layer graphene can be transferred onto another clean SiO_2/Si substrate and the top as-coated PMMA layer can be dissolve quickly by putting the sample directly into

http://dx.doi.org/10.5772/55821

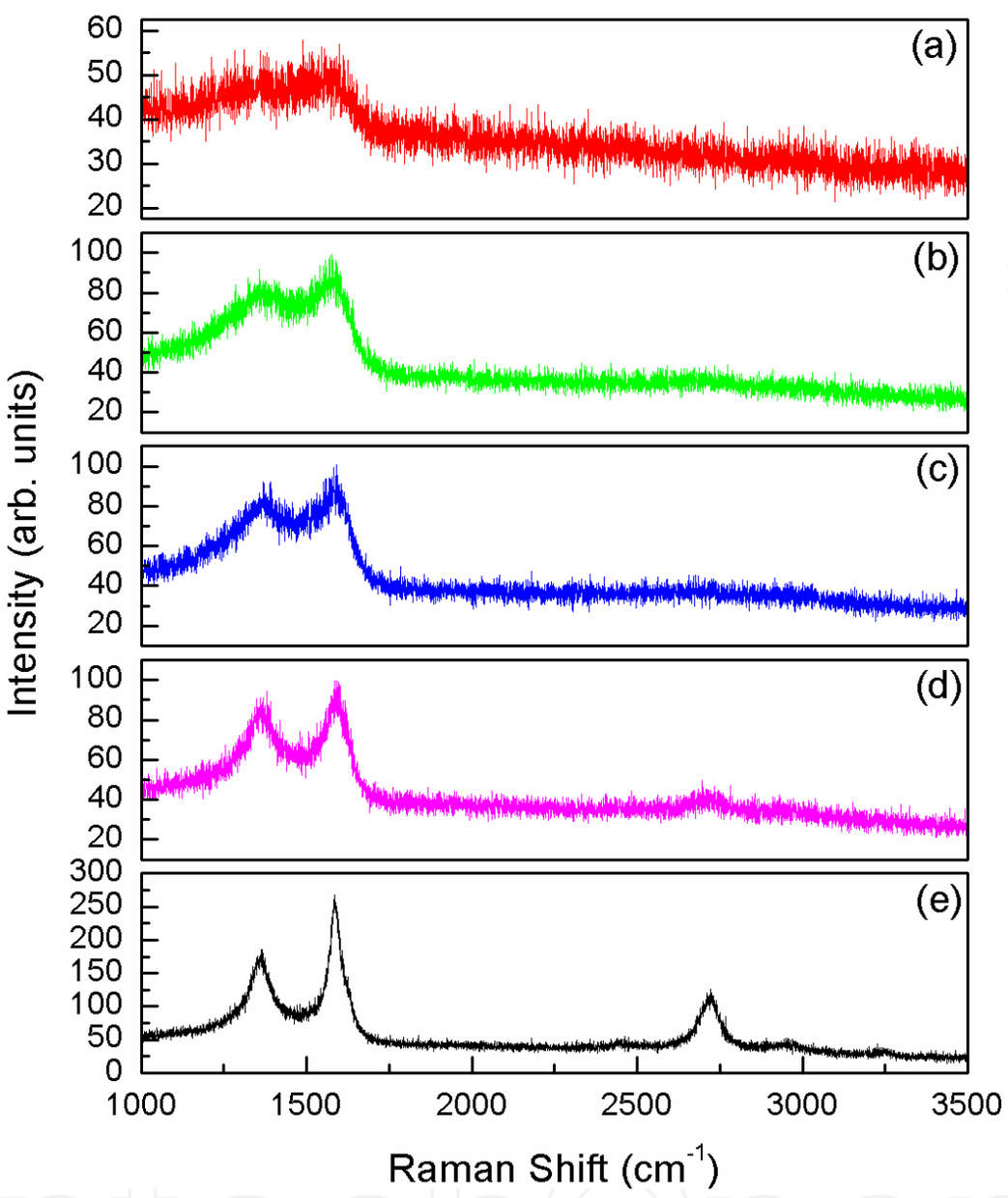

Figure 6. Temperature dependent Ni-induced few layer graphene formation. (a) at 300 °C. (b) at 400 °C. (c) at 500 °C. (d) at 600 °C and (e) at 650 °C.

acetone. The corresponding photographic picture of such graphene layer on the SiO2/Si substrate after successful transfer is shown in figure 8(b). Moreover, the graphene sample preparation method for the transmission electron microscopy (TEM) characterization is slightly different. In this case, after the sample is closely attached to the TEM copper grid, the PMMA can be dissolved by exposing to the acetone vapor for approximately 4 to 5 hours. This transfer process allows maintaining the continuity of the graphene. Figure 8(c) displays the feature of the few-layer graphene and the blue dotted circle denotes the presence of the graphene wrinkles. The formation is primarily due to lattice mismatch between Ni and C and the wrinkles have high possibility to be found at the grain boundaries of as-prepared Ni thin

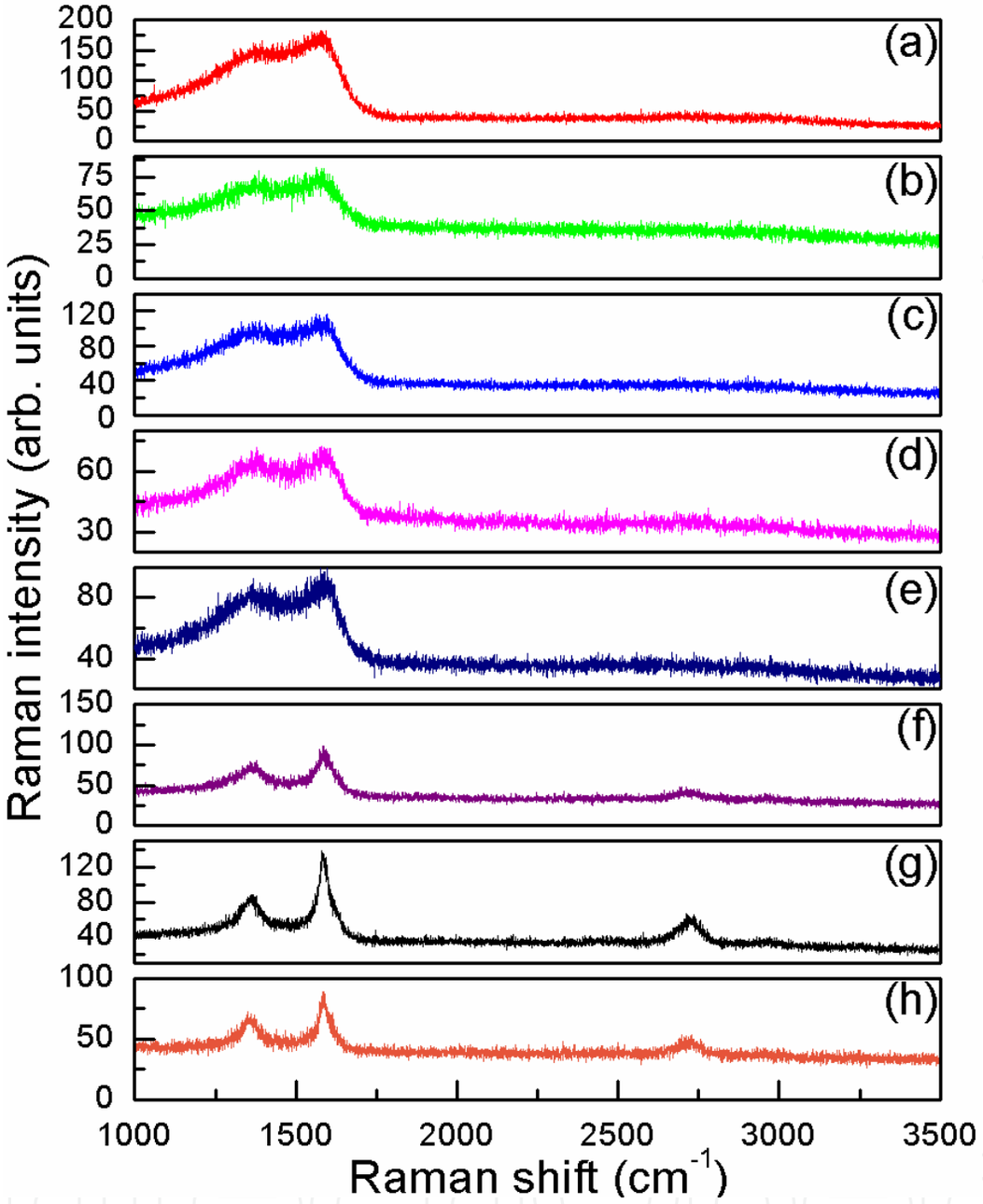

Figure 7. Temperature dependent Co-induced few layer graphene formations. (a) at 300 °C. (b) at 350 °C. (c) at 400 °C. (d) at 450 °C and (e) at 500 °C. (f) at 550 °C. (g) at 600 °C. (h) at 650 °C.

films. Similar with CVD technique, the morphology of fabricated graphene tend to replicate the one of substrate materials. At the edge of the sample which is shown in figure 8(d), the graphene layer by layer feature can be clearly observed. In figure 8(e), the hexagonally symmetric selected area electron diffraction (SADP) for this few-layer graphene was captured indicating the monocrystalline structure of our fabricated few-layer graphene. Two red dotted circles highlight the presence of (0002) lattice plane in the d space. This diffracted spots only appear when few layer or bulk graphite is encountered.

http://dx.doi.org/10.5772/55821

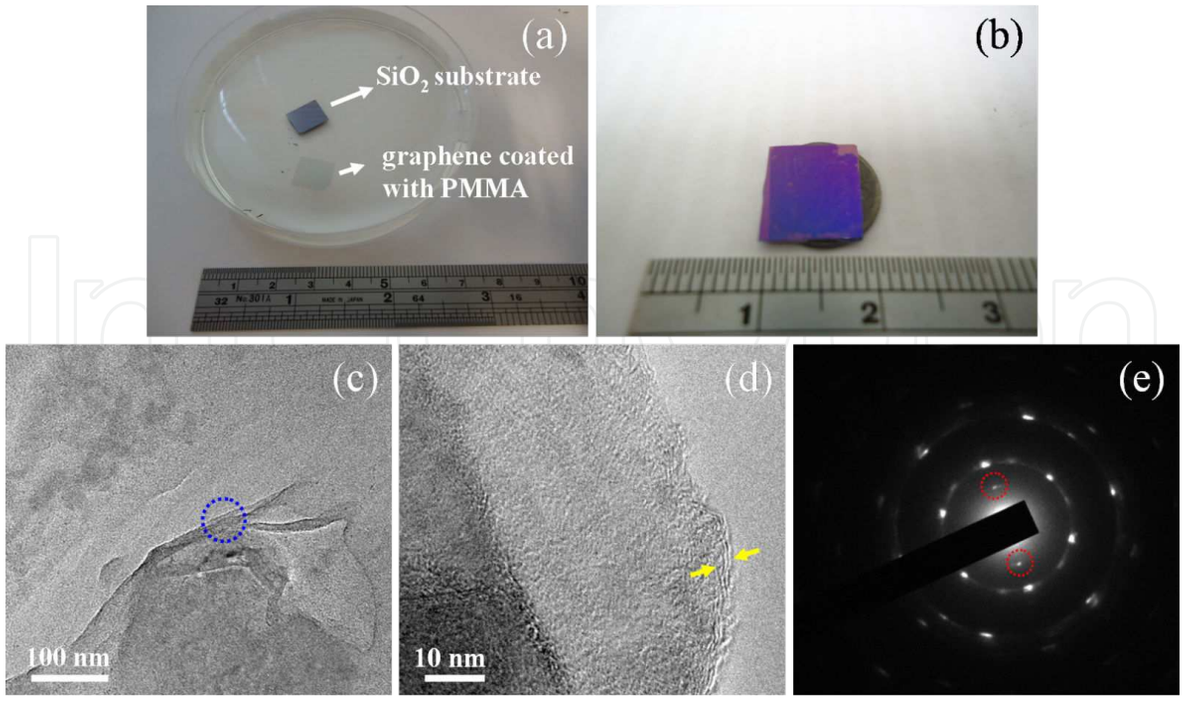

Figure 8. Graphene transfer process after PLD fabrication. (a) Detach of graphene layer from the substrate. (b) Graphene is transferred onto a new piece of SiO_2/Si substrate. (c) Low magnification TEM image shows graphene wrinkles. (d) High resolution TEM image shows few layer graphene edges. (e) The corresponding selected area electron diffraction pattern of few layer graphene.

The high resolution TEM crossing sectional view of bi- and tri- layer graphene are displayed in figure 9(a) and (b) respectively. During the deposition of C at 650 °C, the interdiffusion between C and Ni leads to the formation of the solid solution. Such interdiffusion proceeds until C reaches its saturation status at this temperature. Once the C saturation status reaches, further deposition of C causes a formation of amorphous C layer. Therefore, a well control of the thickness ratio between C and Ni is crucially important in achieving a high quality, bi-, tri- and few layer graphene. When C saturation status reaches at 650 °C, the natural reduction of the substrate temperature to room temperature in high vacuum causes the decrease in the Ni solubility. For this reason, C atoms segregate from the solid solution and form a crystalline and continue graphene layer on the most top of the sample. Figure 9(c) shows the AFM image of the bi-layer graphene. After scratching the sample for depth profile measurement, some graphene parts fold and the relative contrast can be seen from this AFM image. A location across the surface of this piece of graphene was randomly chosen and the corresponding depth profile is shown in figure 9(d). The lateral height which is around 2.5 nm indicates the presence of bi-layer graphene.

Further studies in fabricating graphene by the PLD include the thickness ratio dependence between Ni and C. In this scheme, we found both the number of graphene layers and the D band can be greatly affected. From the Raman spectra in figure 10, C with 3 different thicknesses or laser ablation time were deposited onto 250 nm Ni thin films at 650 °C. The D band is the greatest among those three when the laser ablation time is 120 s (figure 10(a). Moreover,

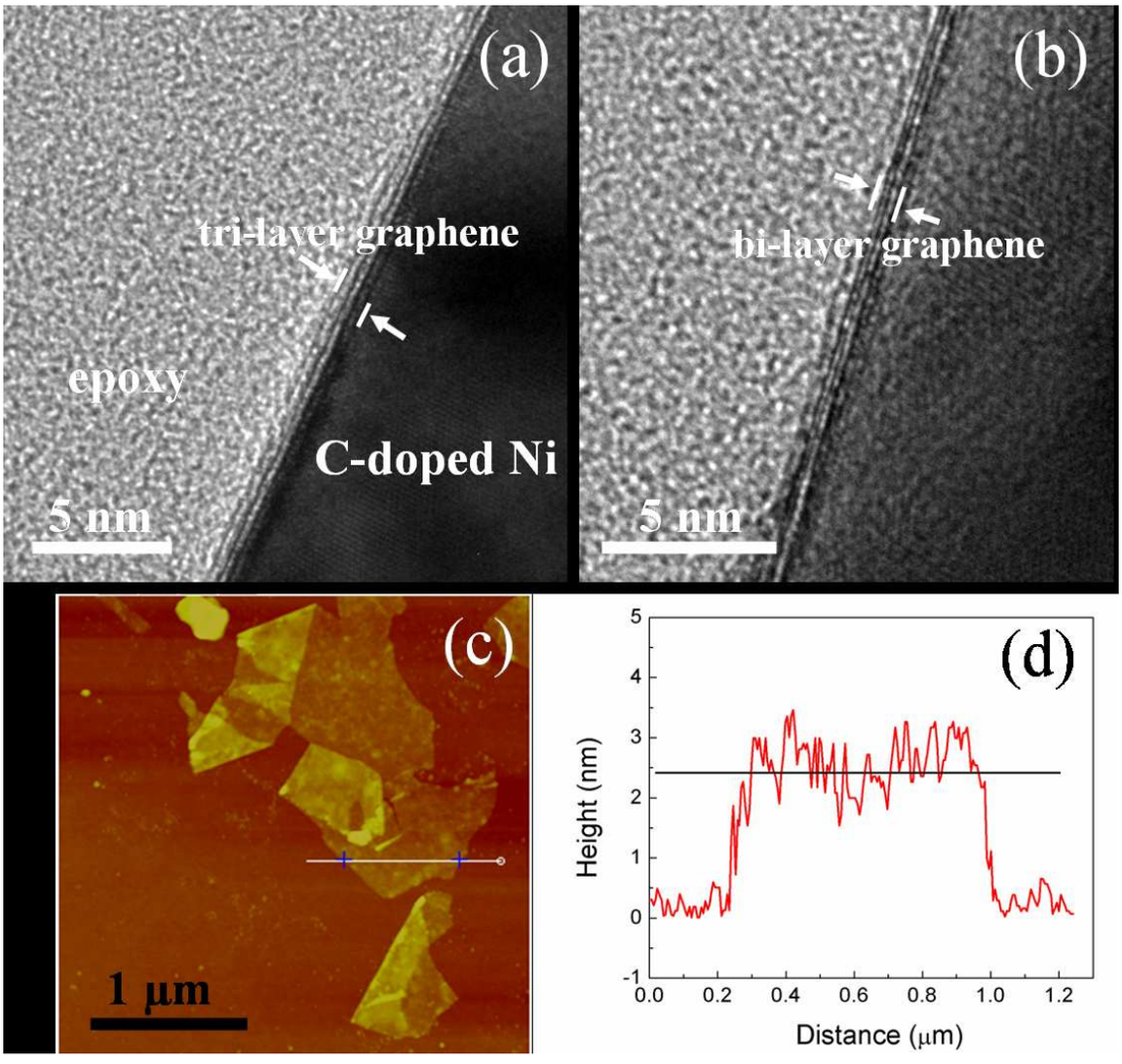

Figure 9. High resolution TEM images show (a) crossing sectional view of tri-layer graphene, (b) crossing sectional view of bi-layer graphene. (c) The AFM image for few layer graphene. (d) The lateral height measurement for few layer graphene.

the intensity ratio of I_{2D}/I_G is 1.24 (Data is summarized in table 1). Thus, both of them imply the poor crystallinity of C layers and the layers. By decreasing the amount of C, such as the resultant Raman spectrum shown in figure 10(b) which corresponds to the laser ablation time of 90 s, the intensity ratio of I_{2D}/I_G is 0.47 which indicates the existence of bi- or tri-layer graphene. Nevertheless, the intensity of the D band is over half of the intensity of the G band. However, when the laser ablation time for C is further decreased to 60 s (figure 10(c)), we observe a significant reduction of the D band Raman intensity and the intensity ratio of I_{2D}/I_G becomes even larger. Similar experiment was done for the graphene fabricated on 250 nm Co thin film. The Raman spectra are shown in figure11 for the different laser ablation times of C, 240 s, 180 s, 120 s, 60 s, and 30 s respectively. The Raman intensities which correspond to each band are summarized in table 2. In contrast to table 1, the graphene which is fabricated on the Co thin film shows similar trend as the laser ablation time for C tends to decrease.

http://dx.doi.org/10.5772/55821

C deposition time (s) / thickness (nm)	D-band position	D-band intensity	G-band position	G-band intensity	2D-band position	2D-band intensity	I_D/I_G	I_{2D}/I_G
120s	1359.30	1011.76	1596.04	814.71	2704.16	130.39	1.24	0.16
90s	1359.30	178.43	1588.48	261.52	2719.27	122.79	0.68	0.47
60s	1346.70	154.17	1580.93	327.43	2688.21	183.99	0.47	0.56

Table 1. Raman intensities for I_D, I_G, I_{2D}, I_D/I_G and I_{2D} / I_G of Figure 10.

C deposition time	D-band position	D-band intensity	G-band position	G-band intensity	2D-band position	2D-band intensity	I_{2D}/I_G
240s	1355.19	358.81	1591.07	403.40	2724.95	97.86	0.24
180s	1355.19	202.91	1581.97	277.00	2724.95	76.17	0.27
120s	1364.30	85.57	1581.97	141.12	2724.95	58.97	0.41
60s	1364.30	65.95	1581.97	113.52	2716.76	55.83	0.49
30s	1364.30	43.17	1581.97	84.08	2707.65	52.29	0.62

Table 2. Raman intensities for I_D, I_G, I_{2D}, I_D/I_G and I_{2D} / I_G of Figure 11.

For the graphene fabricated by the PLD method, the D and 2D bands of bi-layer graphene show some unique characteristics by comparing with few-layer graphene and bulk graphite. As we can see from figure 12(a), the D band of bi-layer graphene possesses a non-symmetric band at 1346.70 cm^{-1} while the few-layer graphene and bulk graphite give symmetric D bands at 1359.30 cm^{-1}. In addition, the Raman spectrum of the asymmetric 2D band of the bi-layer graphene shows red shift relative the ones of few-layer graphene and bulk graphite. Such 2D mode of the bi-layer graphene composes of 4 components, $2D_{1B}$, $2D_{1A}$, $2D_{2A}$, and $2D_{2B}$; in which, $2D_{1A}$ and $2D_{2A}$ have higher intensities than the other two, as shown in figure 12(b). These four components of bi-layer graphene are attributed to the evolution of the electronic band structure. Raman scattering is a fourth order process involving four virtual transitions: [1] a laser induced excitation of an electron-hole pair; [2] electron-phonon scattering with an exchanged momentum; [3] electron phonon scattering with an exchanged momentum; and [4] electron-hole recombination. Based on both TEM and Raman spectroscopic studies, the graphene which is fabricated by the PLD method can be achieved. Nevertheless, there are still some aspects have to be encountered. As we have discussed previously, the number and the quality of graphene layers are decisive by the ratio between C layer and catalytic metals, substrate temperature and laser operation conditions. In order to obtained desirable property of graphene, careful understandings of the graphene and metal interaction, interdiffusion and interface property are crucial.

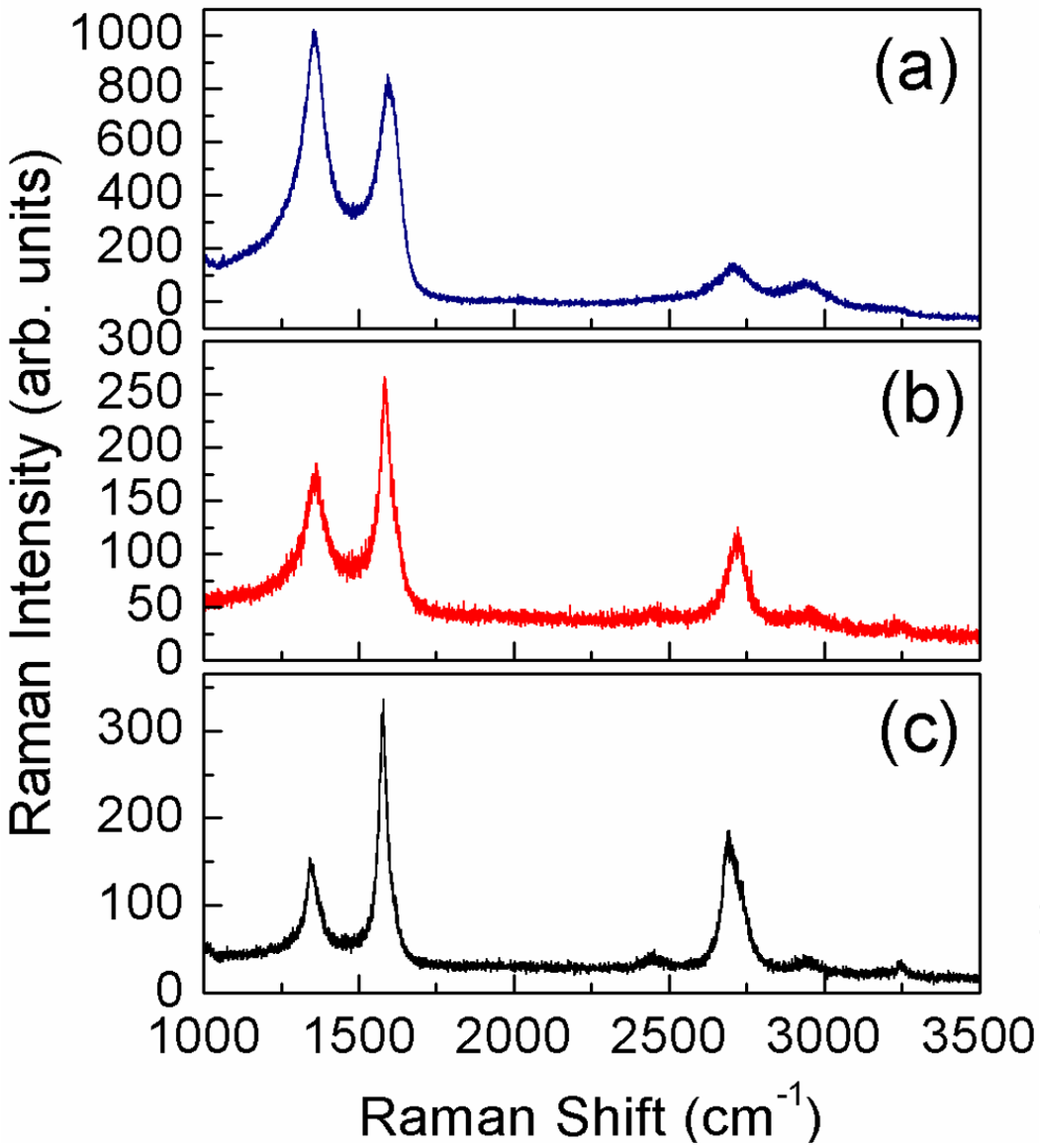

Figure 10. Raman spectroscopic study of different laser ablation time for C deposited onto 250 nm Ni thin film at 650 °C. The corresponding quantities of Raman intensities for each spectrum are summarized in table 1. (a) 120 s laser ablation time. (b) 90 s laser ablation time. (c) 60 s laser ablation time.

http://dx.doi.org/10.5772/55821

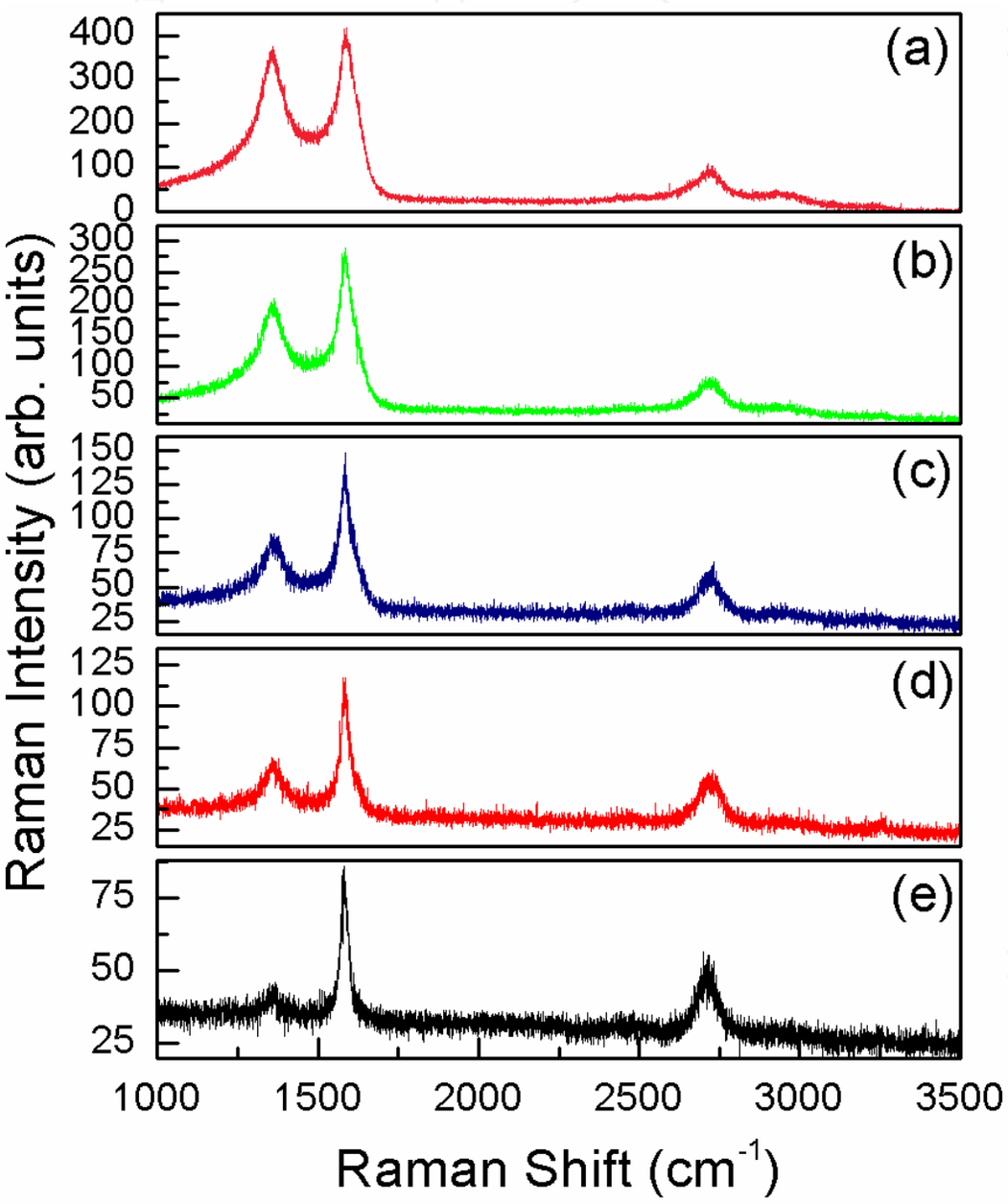

Figure 11. Raman spectroscopic study of different laser ablation time for C deposited onto 250 nm Co thin film at 650 °C. The corresponding quantities of Raman intensities for each spectrum are summarized in table 2. (a) 240 s laser ablation time. (b) 180 s laser ablation time. (c) 120 s laser ablation time. (d) 60 s laser ablation time. (e) 30 s laser ablation time.

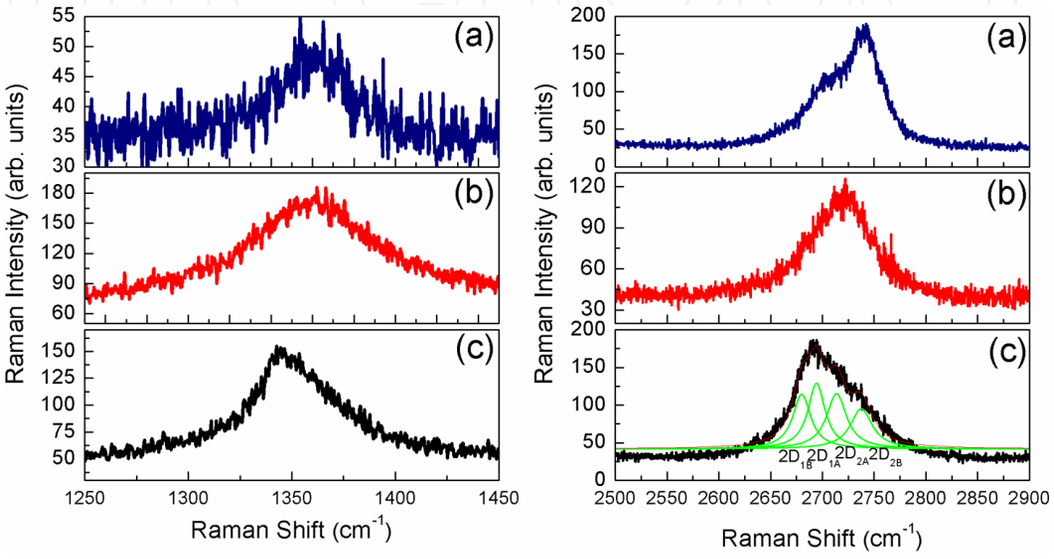

Figure 12. The D and 2D bands for graphene fabricated on Ni thin film by the PLD method.

By the PLD method, other nanostrcutural materials, for instance crystalline Si nanodots, can also be fabricated together with single or multi-layer graphene. Because it is possible to place multi-target within a PLD system, crystalline Si nanodots can then be fabricated via Ni-induced crystallization method as well.[27] Figure 13 (a) and (b) show the SEM images of the crystalline Si nanodots fabricated on top of the graphene layer via the PLD method. Owing to the fact that Si usually required much higher processing temperature (>1000 °C) to be completely crystallized, it has experimentally demonstrated that metal induced crystallization method can reach the same goal with relatively low temperature (< 500 °C). Such kind of Si nanodots structure combined with graphene is very attractive and interesting for studying semiconductor-graphene interface property and eventually reaching the purpose of modern nanoelectronic device design. With regard of such nanostruture, an additional template is necessary in order to define the wide distribution of the Si nanodots. Therefore, a so-called ultra-thin anodic porous alumina (UAPA) template was used in this case. However, the photolithographic and electron beam lithographic techniques can also be applied to graphene. Apparently, it

inevitably proves the functionality of PLD based graphene fabrication method in today's graphene research field.

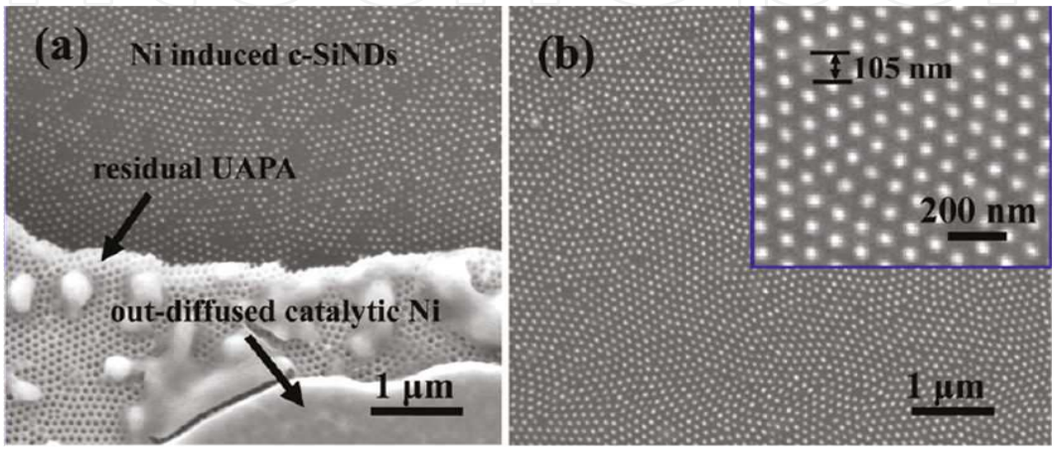

Figure 13. a) Top-view FESEM image of the Ni-induced crystalline silicon nanodots on graphene with remaining UAPA template. (b) The well-ordered nanodots arrays on graphene after lift-off.

5. Conclusion

In this chapter, PLD method has been reviewed for graphene fabrication in this chapter. The foundation of this technique is metal-induced crystallization mechanism. Some catalytic metals need to participate during the crystallization process of C. The advantage of using PLD is to prompt C atoms diffuse into metal thin film at a certain high temperature because PLD can generate high energetic species. After the sample is cooled down, the C atoms segregate from the carbon-metal solid solution and subsequently forming a continuous C thin layer on the top of a carbon containing metal film. The number graphene layer can be controlled by the PLD method, for example by tuning the number of laser pulses, the thickness ratio of C to metal thin film. Besides, we also see the Raman spectroscopy and TEM are both important in characterizing the as-prepared graphene made by the PLD technique. It is expected that PLD based graphene fabrication technique is very promising in current graphene related nano-technology research.

Author details

Kai Wang*

Address all correspondence to: vitalykaiwang@gmail.com

NanoElectronics Group, MESA+ Institute for Nanotechnology, University of Twente, Enschede, The Netherlands

References

[1] I. A. Luk'yanchuk and Y. Kopelevich, Phys. Rev. Lett. 93, 166402 (2004).

[2] K. S. Novoselov, A. K. Geim, S. V. Morozov, D. Jiang, Y. Zhang, S. V. Dubonos, I. V. Grigorieva, and A. A. Firsov, Science 306, 666 (2004).

[3] Y. Zhang, Y.-W. Tan, H. L. Stormer, and P. Kim, Nature 438, 201 (2005).

[4] I. Meric, M. Y. Han, A. F. Young, B. Ozyilmaz, P. Kim, and K. L. Shepard, Nat. Nano. 3, 654 (2008).

[5] X. Li, W. Cai, J. An, S. Kim, J. Nah, D. Yang, R. Piner, A. Velamakanni, I. Jung, E. Tutuc, S. K. Banerjee, L. Colombo, and R. S. Ruoff, Science 324, 1312 (2009).

[6] A. Reina, X. Jia, J. Ho, D. Nezich, H. Son, V. Bulovic, M. S. Dresselhaus, and J. Kong, Nano Lett. 9, 3087 (2009).

[7] R. Hawaldar, P. Merino, M. R. Correia, I. Bdikin, J. Gracio, J. Mendez, J. A. Martin-Gago, and M. K. Singh, Sci. Rep. 2, 1 (2012).

[8] Z. Luo, Y. Lu, D. W. Singer, M. E. Berck, L. A. Somers, B. R. Goldsmith, and A. T. C. Johnson, Chem. Mater. 23, 1441 (2011).

[9] W. K. Kim, Y. M. Jung, J. H. Cho, J. Y. Kang, J. Y. Oh, H. Kang, H. Lee, J. H. Kim, S. Lee, H. J. Shin, J. Y. Lee, Y. C. Kim, I. T. Han, J. M. Kim, J. Yook, S. Baik, and S. C. Jun, App. Phys. Lett. 97, 193103 (2010).

[10] L. s. M. A. Perdigão, S. N. Sabki, J. M. Garfitt, P. Capiod, and P. H. Beton, J. Phys. Chem. C 115, 7472 (2011).

[11] K. Wang, G. Tai, K. H. Wong, S. P. Lau, and W. Guo, AIP Advances 1, 022141 (2011).

[12] J. C. Hamilton and J. M. Blakely, Surf. Sci. 91, 199 (1980).

[13] J. T. Grant and T. W. Haas, Surf. Sci. 21, 76 (1970).

[14] A. T. T. Koh, Y. M. Foong, and D. H. C. Chua, App. Phys. Lett. 97, 114102 (2010).

[15] A. C. Ferrari, J. C. Meyer, V. Scardaci, C. Casiraghi, M. Lazzeri, F. Mauri, S. Piscanec, D. Jiang, K. S. Novoselov, S. Roth, and A. K. Geim, Phys. Rev. Lett. 97, 187401 (2006).

[16] A. C. Ferrari and J. Robertson, Phys. Rev. B 64, 075414 (2001).

[17] F. Tuinstra and J. L. Koenig, J. Chem. Phys. 53, 1126 (1970).

[18] K. Wang and K. H. Wong Semi. Sci. and Tech. 26, 095031 (2011).

[19] J. Wintterlin and M. L. Bocquet, Surf. Sci. 603, 1841 (2009).

[20] K. Wang and K. H. Wong, MRS Online Proceedings Library mrss11-1321-a, 06 (2011).

[21] M. Zheng, K. Takei, B. Hsia, H. Fang, X. Zhang, N. Ferralis, H. Ko, Y. Chueh, Y. Zhang, R. Maboudian, and A. Javey, App. Phys. Lett. 96, 063110 (2010).

[22] M. N. R. Ashfold, F. Claeyssens, G. M. Fuge, and S. J. Henley, Chem. Soc. Rev. 33, 23 (2004).

[23] A. A. Voevodin and M. S. Donley, Sur. Coat. Tech. 82, 199 (1996).

[24] H. M. Smith and A. F. Turner, Appl. Opt. 4, 147 (1965).

[25] D. Dijkkamp, T. Venkatesan, X. D. Wu, S. A. Shaheen, N. Jisrawi, Y. H. Min-Lee, W. L. McLean, and M. Croft, App. Phys. Lett. 51, 619 (1987).

[26] D. P. Norton, in Pulsed Laser Deposition of Thin Films (John Wiley & Sons, Inc., 2006).

[27] G. Tai, K. Wang, Z. Sun, J. Yin, S. M. Ng, J. Zhou, F. Yan, C. W. Leung, K. H. Wong, W. Guo, and S. P. Lau, J. Phys. Chem. C 116, 532 (2011).

IntechOpen